

Distribution of energy-momentum tensor around static quarks in SU(3) gauge theory at high temperature

Enkhtuya Galsandorj,* Sodbileg Chagdaa, Battogtokh Purev and Munkhzaya Batgerel

Laboratory of Theoretical and High Energy Physics, Institute of Physics and Technology, Mongolian Academy of Sciences,

Peace Ave. 54b, 13330 Ulaanbaatar, Mongolia

E-mail: enkhtuyag@mas.ac.mn, sodbilegch@mas.ac.mn, battogtokhp@mas.ac.mn, munkhzayab@mas.ac.mn

In this study, we explore the distribution of energy-momentum tensor around a static quark and an antiquark in SU(3) pure gauge theory at finite temperature. Double extrapolated transverse distributions on mid-plane of the flux tube have been presented for the first time at nonzero temperature. Also, we investigate the spatial distributions of the flux tube on the source plane obtaining from the stress tensor for several $q\bar{q}$ separations and temperatures above and below the critical temperature. The resultant distributions show the detailed structure of the flux tube. Finally, we show the dependence of F_{stress} that is computed from the integral of the stress tensor on the distance between the quark and antiquark on a finer lattice.

*The 39th International Symposium on Lattice Field Theory,
8th-13th August, 2022,
Rheinische Friedrich-Wilhelms-Universität Bonn, Bonn, Germany*

*Speaker

1. Introduction

In QCD, the study of thermodynamical quantities such as energy, pressure and entropy density is important to describe the quark confinement phenomenon, study the properties of quark-gluon plasma and understand the physics of the particles from a relativistic heavy ion-collisions. The most convenient method to study these thermodynamical quantities is to formulate the energy-momentum tensor (EMT) $T_{\mu\nu}$ ($\mu, \nu = 1, 2, 3, 4$). Once the energy-momentum tensor has been computed, the thermodynamical quantities can be obtained from the components of the tensor and their correlators. For example, in Euclidean space the components of the EMT are related to the physical quantities as follows

$$-T_{44}(x) = \varepsilon(x) \quad (\text{Energy density}), \quad (1)$$

$$T_{\mu\nu}(x) = \sigma_{\mu\nu}(x), \quad (\mu, \nu = 1, 2, 3) \quad (\text{Stress tensor}), \quad (2)$$

$$T_{\mu\mu}(x) = p(x), \quad (\mu = 1, 2, 3) \quad (\text{Pressure}), \quad (3)$$

and the correlator quantities are important to study the bulk and shear viscosities at nonzero temperature. Moreover, the tensor is suitable to investigate the local and global properties of the field.

On the lattice, discretization of the EMT was challenging problem, because when one goes to continuum physics, observables do not correspond to continuum due to UV-fluctuation. Therefore, until recently, researchers used the ‘‘integral method’’ [1] which is an indirect method to calculate thermodynamical observables such as energy density and pressure. In 2010, however, the gradient flow method [2, 3] was introduced into the lattice field theory, making it possible to formulate EMT on the lattice. The formulation of the EMT on the lattice using the gradient flow method was developed by Japanese physicists for the first time in 2013 [4]. And, distributions of the EMT around a quark and an antiquark have been determined in Ref.[5] at zero temperature and in Ref.[6] at nonzero temperature. Also, the distributions of the EMT for the single quark system have been computed in the deconfined phase [7]. Although, in Ref.[6] the distributions have been computed only at one temperature, and the continuum limits have not been taken for the $q\bar{q}$ system at finite temperature.

For that reason, in this study we investigated the distribution of the flux tube at several temperatures around the critical temperature and for the shorter and longer distances between the quark and antiquark, and did double extrapolation.

The plan of the paper is the following: in Section 2 we recall theoretical background of the energy-momentum tensor and its definition on the lattice. And the method and simulation details will be shown. In Section 3, we introduce our results and findings, and finally the conclusion will be included in Section 4.

2. Theory and method

The energy-momentum tensor consists of gauge and fermionic part in continuum as

$$T_{\mu\nu}(x) = T_{\mu\nu}^G(x) + T_{\mu\nu}^F(x). \quad (4)$$

In this study we only focus on the gauge part which is constructed from field strength tensor $F_{\mu\rho}^a$ of the gluon field, $T_{\mu\nu}^G(x) = \frac{1}{g_0^2} [F_{\mu\rho}^a(x)F_{\nu\rho}^a(x) - \frac{1}{4}\delta_{\mu\nu}F_{\rho\sigma}^a(x)F_{\rho\sigma}^a(x)]$, where g_0 is bare gauge coupling. As mentioned in Introduction section, we formulate the energy-momentum tensor using the gradient flow method. The main concept of the method is to introduce the extra fifth coordinate named flow time t on the four-dimensional space-time lattice. Then one can measure the observables on the non-zero and positive value of the flow time. For the EMT operator, the small- t expansion method determined from the gradient flow method was used. In this method, the observables are defined by the sum of the flowed operators. For the energy-momentum tensor, these operators are E and U operators and the EMT is given in terms of these operators as

$$T_{\mu\nu}(t, x) = c_1(t)U_{\mu\nu}(t, x) + 4c_2(t)E(t, x), \quad (5)$$

and E and U operators built-up from the flowed field strength tensor $G_{\mu\rho}^a(t, x)$ in the following form

$$U_{\mu\nu}(t, x) = G_{\mu\rho}^a(t, x)G_{\nu\rho}^a(t, x) - \frac{1}{4}G_{\rho\sigma}^a(t, x)G_{\rho\sigma}^a(t, x), \quad (6)$$

$$E(t, x) = \frac{1}{4}G_{\rho\sigma}^a(t, x)G_{\rho\sigma}^a(t, x), \quad (7)$$

and c_1 and c_2 are the flow time dependent perturbative coefficients [8, 9]. Then, the renormalized continuous EMT can be extracted by taking the double limit

$$T_{\mu\nu}^R(x) = \lim_{t \rightarrow 0} \lim_{a \rightarrow 0} T_{\mu\nu}(t, x). \quad (8)$$

Now, let's discuss how to measure the EMT around the quark-antiquark system. At finite temperature, we consider the EMT operator given by Eq.(5) and Polyakov loop correlation function [6]

$$\langle T_{\mu\nu}(t, x) \rangle_{q\bar{q}}^{lat} = \frac{\langle T_{\mu\nu}(t, x) \mathbf{Tr} [L^\dagger(0)L(R)] \rangle}{\mathbf{Tr} [L^\dagger(0)L(R)]} - \langle T_{\mu\nu}(t, x) \rangle. \quad (9)$$

Here two Polyakov loops, $L(\vec{n}) \equiv \frac{1}{N_c} \text{Tr} \prod_{\tau=1}^{N_\tau} U_4(\vec{n}, \tau)$, indicate the positions of the quark and antiquark R -spaced from each other.

In Fig.(1), we want to show the planes in which the distributions of the EMT around the $q\bar{q}$ are studied, where (z, x) plane that including the quarks and (x, y) plane is the middle transverse plane between the quark and antiquark. In order to study the distribution on middle plane, we transfer from

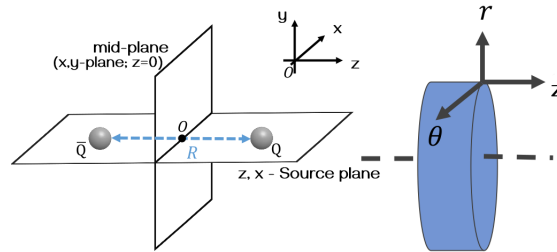


Figure 1: left: The sketch of the $q\bar{q}$ system, right: cylindrical coordinate [10].

the Cartesian coordinate system to the cylindrical because of the cylindrical symmetry behavior of

the flux tube. The transformation is given by the following equation

$$T_{\gamma\gamma'} = (e_\gamma)_\mu T_{\mu\nu} (e_{\gamma'})_\nu, (\gamma\gamma' = r, \theta, z), \quad (10)$$

$$r = \sqrt{x^2 + y^2}, \theta = \tan^{-1}\left(\frac{y}{x}\right), z = z$$

where e_γ denotes a unit vector along the direction of the γ axis. Consequently, the EMT on the middle plane between the quarks is diagonalized as

$$T_{\gamma\gamma'}(r) = \text{diag}(T_{44}(r), T_{rr}(r), T_{\theta\theta}(r), T_{zz}(r)). \quad (11)$$

Then, in order to extract the renormalized energy-momentum tensor we need to do double extrapolation that are continuum ($a \rightarrow 0$) and zero-flow time ($t \rightarrow 0$) limits. First the continuum limit is taken as

$$\langle T_{\mu\nu}(t, x) \rangle_{lat} = \langle T_{\mu\nu}(t, x) \rangle_{cont} + \frac{b_{\mu\nu}(t)}{N_\tau^2}, \quad (12)$$

by fixing the temperature, $q\bar{q}$ separation and flow time in their physical units [11]. After the zero-flow time limit is taken as

$$\langle T_{\mu\nu}(t, x) \rangle_{cont} = \langle T_{\mu\nu}^R(x) \rangle + C_{\mu\nu}(t) \cdot t,$$

using the continuum limited operators obtained for every fixed flow time [11].

The simulation parameters and conditions are shown in Tab.(1). We measure the EMT distri-

T/T_c	$N_\sigma^3 \times N_\tau$	tT^2	a , fm	R , fm	N_{conf}
0.95	$32^3 \times 8$	0.003 - 0.007	0.086	0.5 - 1.2	1000
	$48^3 \times 12$	0.003 - 0.007	0.058	0.5 - 0.9	1000
	$64^3 \times 16$	0.003 - 0.007	0.044	0.5 - 0.9	500
	$96^3 \times 20$	0.003 - 0.007	0.035	0.5 - 0.8	250
1.44	$32^3 \times 8$	0.005 - 0.014	0.057	0.5 - 0.9	1000
	$48^3 \times 12$	0.005 - 0.014	0.038	0.5 - 0.8	1000
	$64^3 \times 16$	0.005 - 0.014	0.029	0.5 - 0.6	500
	$96^3 \times 20$	0.005 - 0.014	0.029	0.4 - 0.6	250

Table 1: Simulation parameters.

bution in SU(3) pure gauge theory at high temperature. In order to take the continuum limit we perform the simulation on the four lattices of different sizes. And we measure the EMT at two temperatures below and above the critical temperature and for several $q\bar{q}$ separations. It should be noted that we measure both EMT and Polyakov loops at nonzero flow time, while in the previous work [6] the EMT have been measured at nonzero flow time and the Polyakov loops have been measured at zero flow time. In order to express the observables in physical units, we use the scaling function that is defined using w_0 quantity [11]. Statistical errors are computed by Jackknife method.

3. Results and discussions

3.1 Stress-tensor distributions on source plane

First, we study the stress tensor distribution on the source plane to investigate the qualitative feature of the flux tube. The stress tensor distribution around the quark and antiquark is obtained

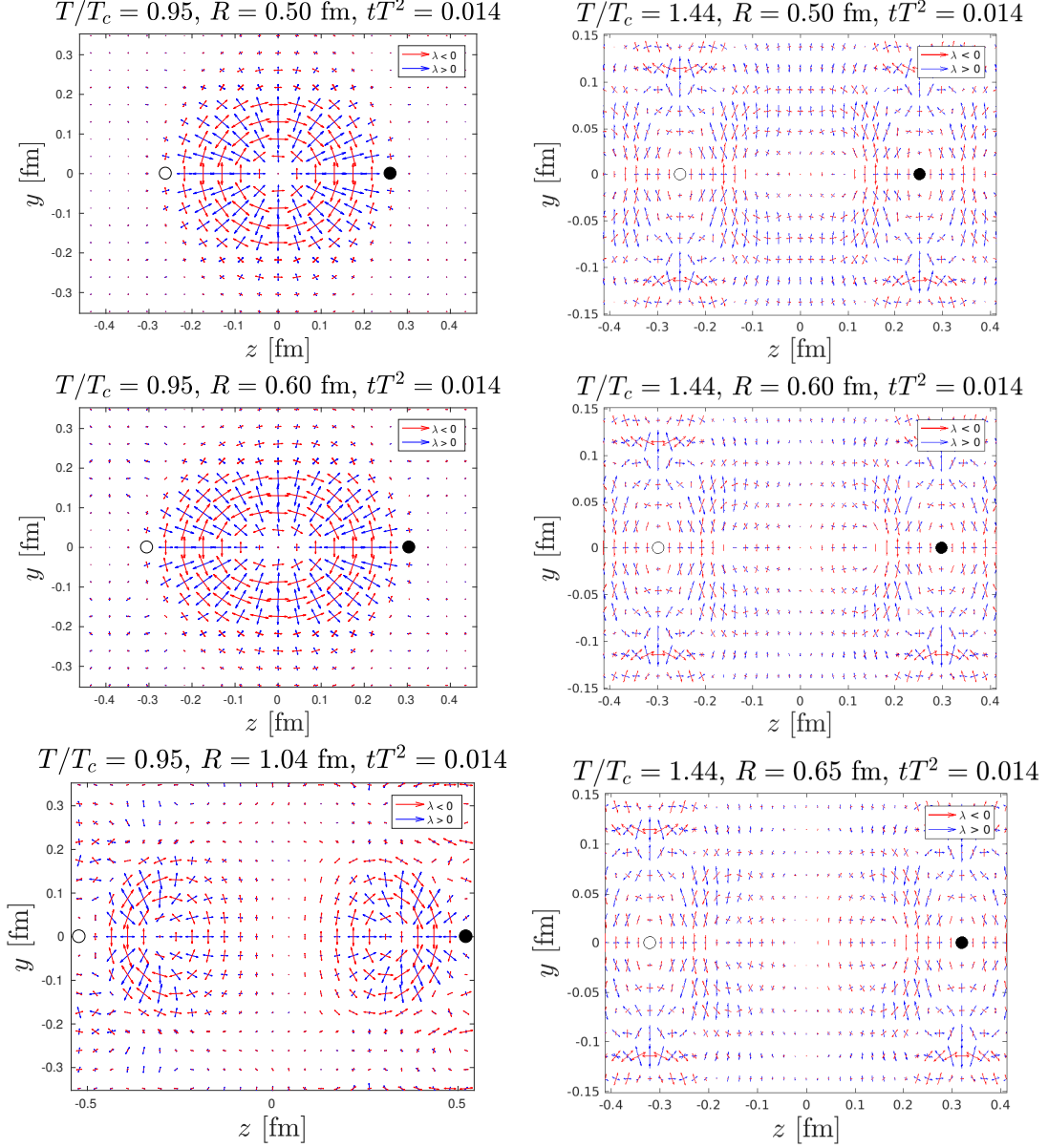


Figure 2: Stress-tensor distributions on the source plane.

by solving eigenvalue equation [5]

$$T_{\mu\nu}n_\nu^{(k)} = \lambda_k n_\mu^{(k)}, (k = 1, 2, 3) \quad (13)$$

where the eigenvalue λ_k is force per unit area along the principal axis and n_ν is normal vector with the surface. When the $\lambda_k < 0$ (red), the pulling strength and $\lambda_k > 0$ (blue), the pushing strength

can be obtained, respectively. The lengths of the arrows are proportional to the absolute value of the eigenvalue and the directions of the arrows are determined by normal vector.

From the Fig.(2), we intended to study the dependence of the field strength lines on temperature and distance between the quarks. We plotted the distributions for three different distances from shorter to longer and at two temperatures below and above T_c on the finer lattices. For the shorter distance, the flux tube can be observed at both temperatures. But, the field strength line's behaviours are different, in other words, for the below critical temperature, there is no field around the positions of the quarks, and for the above T_c , the field strength lines around the quarks are seen. For $T = 0.95T_c$ and $R = 0.5$ fm, the flux tube structure is similar to the flux tube at zero temperature [5]. In the second row of Fig.(2), the stress tensor distributions have been plotted for the 0.6 fm distance and at also two temperatures. From these plots, the flux tube structure still persists at temperature below T_c , but for the above T_c , the flux tube is beginning to dissociate from the middle. In the last row of the figure, the distributions are shown for the longer distance between the sources, at $0.95T_c$, $R = 1.0$ fm and at $1.44T_c$, $R = 0.65$ fm. In both plots the flux tube structure disappeared. But field strength line's behaviors are different. For the below T_c , it seems like become a string breaking and then two new flux tubes emerged, but for the above T_c , there is no interaction between the quark and antiquark, and field strength lines around the quarks become like two separated point charge's field. The stress tensor distribution's formation at $T = 1.44T_c$ and $R = 0.65$ fm is similar to that of the Ref.[6] in which the temperature and the distance were $1.44T_c$ and $R = 0.69$ fm.

3.2 Double extrapolated EMT distribution on mid-plane

Next, we study the distribution of the energy-momentum tensor on the middle plane. In order to do we move to cylindrical coordinate using Eq.(10), and then the double extrapolation is taken according to Eq.(12) and Eq.(13). Firstly, we did the extrapolations for only one point of the components at $(z = 0, r = 0)$, and it is illustrated in the first row of Fig.(3). It should be noted that we did not include the systematic errors here, and only statistical errors are considered. Then we have to do the above operation for all points of the the transverse distribution. In order to take the continuum limit, we need the data at same r for different lattices. Since values of the r are different on the various lattice extends, we have to parametrize the transverse profile using following functions [12] and [13]

$$F_{Gauss} = A \cdot e^{-Br^2} + C, \quad (14)$$

$$F_{Bessel} = A \cdot K_0(\sqrt{Br^2 + C}). \quad (15)$$

After the parametrization, we can get the data at arbitrary r . In this study, we use values of the r on the finest lattice. Once it is done, we repeat the steps that are performed for one point. The second row of Fig.(3), we show the dependence of the transverse distribution of the energy density on $1/N_\tau^2$ and tT^2 with the continuum and the zero-flow time limited results as an example. In Fig.(4), we show the double extrapolated components of the EMT on the middle plane at two temperatures and for two distances. From these figures, we can see that $-\langle T_{44}^R(r) \rangle_{q\bar{q}}/T^4$ or energy density has a much larger value than that of the other three components. And $-\langle T_{zz}^R(r) \rangle_{q\bar{q}}/T^4$ component of the EMT, in other words, the component along the axis connecting quarks has a higher value than that of the other space-space components for the small separation $R = 0.5$ fm in the confined

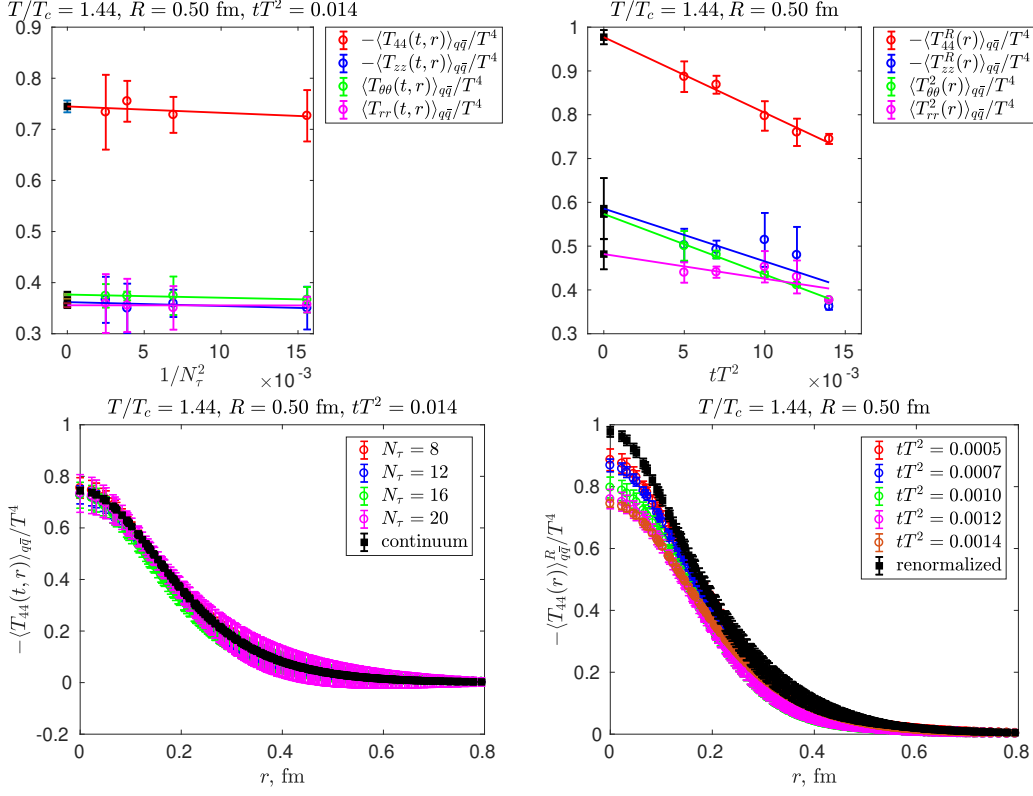


Figure 3: Dependence of the components of the EMT on N_τ and flow time t with the continuum and zero-flow time extrapolated points. Top: at $(z = 0, r = 0)$ point, Bottom: on the middle plane $(z = 0, r)$.

phase. But, for the larger separation, it decreases and has a similar value to the other two space-space components. Besides, when the distance increases, the values of the components decrease. For the temperature dependence, when the distance is fixed and the temperature is increased, the values of all components are decreased and approach zero. Also, the difference between the energy density and the space-space components decreases.

3.3 $q\bar{q}$ force

Before, in Ref.[5], it has been shown that the $q\bar{q}$ force can be evaluated by the stress-tensor distribution and coincides with the $q\bar{q}$ force from the potential at zero temperature. Therefore, we investigate the dependence of the $q\bar{q}$ force on the distance between the quarks from the distribution of the stress-tensor surrounding the charges. It is computed by the surface integral

$$F_{stress} = - \int_S T_{\mu\nu} dS_j = 2\pi \int_0^\infty \langle T_{zz}(r, t) \rangle_{q\bar{q}} r dr \quad (16)$$

surrounding the charge and for the surface, we choose the distribution of the $\langle T_{zz}(r, t) \rangle_{q\bar{q}}$ component at mid-plane [5]. In Fig.5, we show the dependence of the $q\bar{q}$ force on the distance between the quarks at two temperatures. From the figure, one can see that the dependence of the force on $q\bar{q}$ separation is different for the two temperatures. In other words, at temperature below T_c , this dependence is similar to that of at zero temperature [5]. But the magnitude of the force is lower

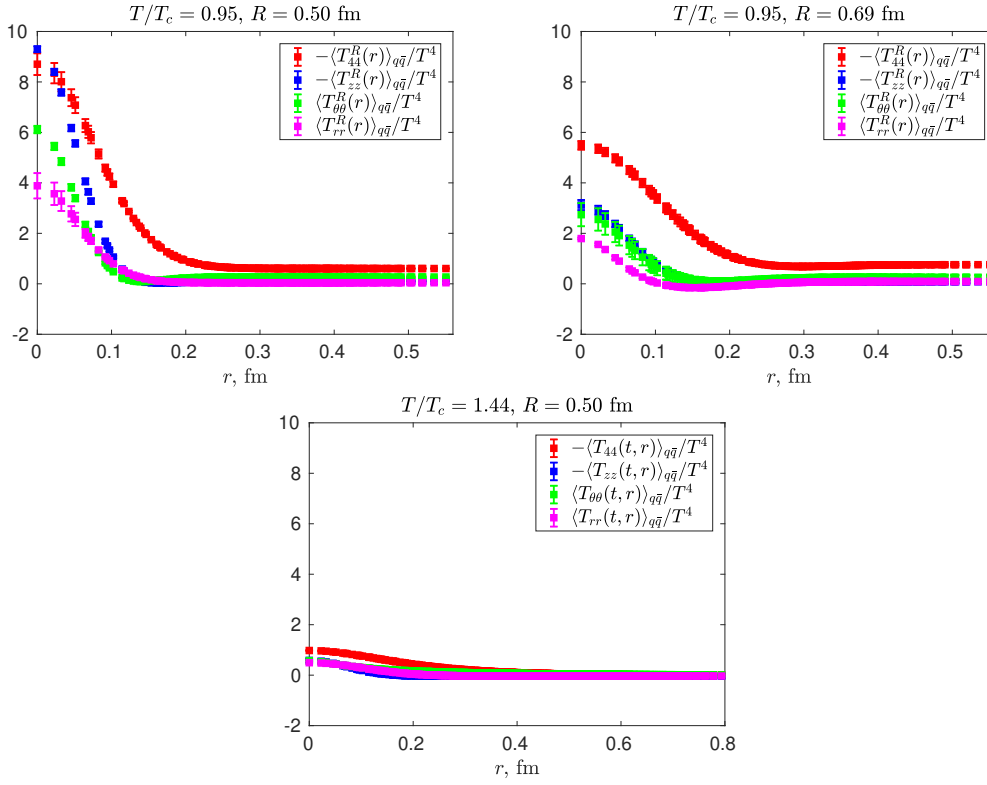


Figure 4: Distributions of double extrapolated components of the EMT on the middle plane as functions of the temperature and the $q\bar{q}$ separation.

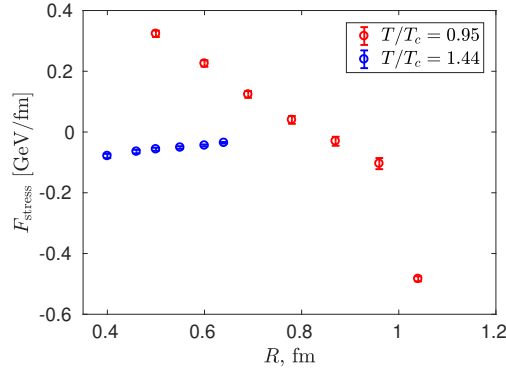


Figure 5: Dependence of the $q\bar{q}$ force on the distance between the quarks at two temperatures.

than that of the vacuum. And, at temperature the above T_c , the dependence is different. Also, the value is decreasing and reaching a zero. From this, we suppose that the screening phenomenon occurs in the deconfined phase.

4. Conclusion

We have studied the distribution of the energy-momentum tensor around a quark and an antiquark at high temperature in the SU(3) pure gauge theory. And we have taken the continuum and the zero-flow time limits for the transverse profile on the mid-plane of the flux tube for the first time at nonzero temperature, successively. From our results and findings, we may make the following conclusions:

- We explicitly illustrate the dissociation of the flux tube at large separation is in a different way for the temperatures below and above critical temperature from stress-tensor distribution on the source plane. This may indicate that the following phenomena are occurring:
 - $T < T_c$: String breaking,
 - $T > T_c$: Color screening.
- As T and R increased, the change of the $T_{zz}^R(r)$ behavior and the decrease of all components show the flux tube disappearance.
- At $T < T_c$, relation between the components was similar to the QCD vacuum and different from the classical electrodynamics, which is turned up from $\langle T_{44}^R(r) \rangle + \langle T_{zz}^R(r) \rangle + \langle T_{\theta\theta}^R(r) \rangle + \langle T_{rr}^R(r) \rangle < 0$. And at $T > T_c$, the relation has changed, which is $\langle T_{44}^R(r) \rangle + \langle T_{zz}^R(r) \rangle + \langle T_{\theta\theta}^R(r) \rangle + \langle T_{rr}^R(r) \rangle \approx 0$.

Acknowledgments

This work was carried out under the project ShuSS-2020/24 in Mongolia. The authors thank colleagues in Bielefeld for the encouragement to develop our branch program using the SIMULATeQCD program [14, 15]. For two coarser lattices, generation of the gauge and flowed configurations, and flux tube measurements have been performed at the Institute of Physics and Technology of Mongolian Academy of Sciences. For two finer lattices, the simulations have been performed on the Bielefeld GPU cluster.

References

- [1] G. Boyd, J. Engels, F. Karsch, E. Laermann, C. Legeland, M. Luetgemeier and B. Petersson, *Thermodynamics of SU(3) Lattice Gauge Theory*, *Nucl.Phys.* **B469** 419 (1996), [hep-lat/9602007].
- [2] M. Luescher, *Properties and uses of the Wilson flow in lattice QCD*, *JHEP* **1008** 071 (2010), [hep-lat/1006.4518].
- [3] M. Luescher and P. Weisz, *Perturbative analysis of the gradient flow in non-abelian gauge theories*, *JHEP* **1102** 051 (2011), [hep-lat/1101.0963].
- [4] H. Suzuki, *Energy-momentum tensor from the Yang-Mills gradient flow*, *Prog. Theor. and Exp. Phys.* **2** 083B03 (2013), [hep-lat/1304.0533].

- [5] R. Yanagihara, T. Iritani, M. Kitazawa, M. Asakawa and T. Hatsuda, *Distribution of stress tensor around static quark-anti-quark from Yang-Mills gradient flow*, *Phys. Lett.* **B789** 210 (2019).
- [6] R. Yanagihara, T. Iritani, M. Kitazawa, M. Asakawa, T. Hatsuda (FlowQCD collaboration), *Stress distribution in quark-anti-quark and single quark systems at nonzero temperature*, *PoS 2019* **004** (2019), [hep-lat/1912.04641].
- [7] M. Kitazawa, R. Yanagihara, M. Asakawa and T. Hatsuda, *Single static-quark system above T_c investigated by energy-momentum tensor in $SU(3)$ Yang-Mills theory*, *PoS 2021* **396** (2021), [hep-lat/2111.15103].
- [8] T. Iritani, M. Kitazawa, H. Suzuki and H. Takaura, *Thermodynamics in quenched QCD: energy-momentum tensor with two-loop order coefficients in the gradient flow formalism*, *Prog. Theor. and Exp. Phys.* **2** 023B02 (2019), [hep-lat/1812.06444].
- [9] R. V. Harlander, Y. Kluth and Fabian Lange, *The two-loop energy-momentum tensor within the gradient-flow formalism*, *Eur.Phys.J.* **C78** 944 (2018), [hep-lat/1808.09837].
- [10] R. Yanagihara, *Distribution of energy momentum tensor around static charges in lattice simulations and an effective model*, *doctoral dissertation* (2021).
- [11] M. Kitazawa, T. Iritani, M. Asakawa, T. Hatsuda and H. Suzuki, *Equation of state for $SU(3)$ gauge theory via the energy-momentum tensor under gradient flow*, *Phys. Rev.* **D 94** 114512 (2016), [hep-lat/1610.07810].
- [12] C. Schlichter, G.S. Bali and K. Schilling, *Color flux profiles in $SU(2)$ lattice gauge theory*, *Nucl. Phys.* **B42** 273 (1995).
- [13] J. R. Clem, *Simple model for the vortex core in a type II superconductor*, *J. Low Temp. Phys.* **18**, 427 (1975).
- [14] L. Mazur, *Topological aspects in lattice QCD*, Ph.D. thesis, Bielefeld University (2021), <https://doi.org/10.4119/unibi/2956493>
- [15] L. Altenkort, D. Bollweg, D. A. Clarke, O. Kaczmarek, L. Mazur, C. Schmidt, P. Scior and H.-T. Shu, *HotQCD on Multi-GPU Systems*, *PoS (LATTICE 2021)* **196** (2021), [hep-lat/2111.10354].